Partial mixing phase of binary cells in finite systems

Danh-Tai Hoang,[1,*] Juyong Song,[1,2] and Junghyo Jo[1,2,†]
[1]*Asia Pacific Center for Theoretical Physics, Pohang, Korea*
[2]*Department of Physics, POSTECH, Pohang, Korea*
(Received 20 August 2013; revised manuscript received 18 November 2013; published 30 December 2013)

We study the self-organization of binary cell mixtures in finite cubic lattices. Depending on the relative attractions between cell types, the binary mixture model generates four distinct cellular associations: complete sorting, shell-core sorting, partial mixing, and complete mixing of heterotypic cells. At the boundaries between these four phases, the cellular associations show large variations, representing phase transitions. We find that the partial mixing phase is highly tolerant to thermal fluctuations. Interestingly, human pancreatic islets, the micro-organs for glucose homeostasis, adapt the partial mixing phase consisting of α and β cells.

DOI: 10.1103/PhysRevE.88.062725 PACS number(s): 87.18.Ed, 89.75.Fb, 87.15.ak

I. INTRODUCTION

Natural materials and systems have specialized structures. Even a simple system with two species can form various patterns. The binary mixture has been intensively studied in physics and chemistry. The physical models generally consider interactions between two species: up and down spins in the Ising model [1], occupied and empty sites in the contact process [2], and binary gases in the lattice gas model [3]. Binary mixtures of lipids and detergent is another example studied in chemistry [4].

The concept of *self-organization* in the binary mixture models has also been used to explain the morphogenesis in biology [5]. Steinberg has proposed the *differential adhesion hypothesis* (DAH) that given adhesion strengths between cell types, the binary cell mixture has an equilibrium structure minimizing its free energy [5]. As an alternative hypothesis, differential cell motility has also been proposed to explain cell sorting in the binary cell mixture [6]. During the past decades, DAH has been confirmed in experiments [7]. In addition, DAH developed different computational models. One simple model is the cellular lattice model in which each site represents a cell. Considered were the 2-dimensional regular square lattice [8], 2-dimensional triangular lattice [9], 3-dimensional cubic lattice [10], and 3-dimensional hexagonal close-packed lattice [11]. Another popular model is the subcellular lattice model, proposed by Graner and Glazier [12,13]. In this model, each cell extends over many contiguous sites on a lattice. Therefore, the model can describe morphological changes of single cells specifically at cell-to-cell contacts. Since the computational cost for updating many sites per cell is high, this model has been considered usually in 2 dimensions [12–14] and rarely extended to 3 dimensions [15]. DAH has also been considered in a centric model and vertex model (reviewed in Refs. [16,17]). In addition to the lattice models, off-lattice and continuous models have been developed to study cell movement [18,19] and cell sorting [11].

Unlike general physical and chemical binary mixture models, the biological model has to consider cellular composition and finite size effect in addition to cellular interactions. Pancreatic islets, consisting of two major cell types, are micro-organs for glucose homeostasis. Persistent elevation of blood glucose levels is defined as the metabolic disease, diabetes. Endocrine α and β cells in the islet play reciprocal roles for increasing and decreasing glucose levels in fast and fed conditions, respectively. In addition, they interact with each other [20,21], although its implication for glucose homeostasis has not been completely understood. Considering their functional interaction, their physical contacts may have physiological implications. In general, an islet contains a few to several thousand endocrine cells [22]. Although the size range of islets is similar between species, the spatial organization of α and β cells looks different between species. In mouse islets, dominant β cells are located in the core, while α cells are surrounded on the periphery. However, human islets contain a higher fraction of α cells, 20%–40%, compared with 10%–20% in mouse islets [22]. In human islets, α cells are not only distributed on the islet periphery, but also scattered within islets [23–25]. Controversial observations have been reported regarding the cell arrangement in human islets. Some reported an organized structure where human islets were subdivided into subunits comprising clusters of β cells surrounded by α cells [25], while others reported a more or less random structure where α and β cells were irregularly distributed throughout human islets [23,24].

To examine the species-dependent structures of pancreatic islets and their potential cell rearrangement under pathological conditions, we systematically study the self-organization of the binary mixture model. In particular, we consider a simple cubic lattice model, which is simple for computation while complex enough to reproduce all the structural aspects of pancreatic islets.

This paper is organized as follows: We describe our model and simulation method in the next section. Then, we show and discuss how cellular interaction and composition govern the self-organization of islets in Secs. III and IV. Finally, we summarize our findings in Sec. V.

II. BINARY MIXTURE MODEL

To understand the spatial organization of binary cells, we consider a lattice model where each site is occupied by either an α or β cell. The relative attractions between cell types are represented by $J_{\alpha\alpha}$, $J_{\beta\beta}$, and $J_{\alpha\beta}$ for α-α, β-β, and α-β

*danh-tai.hoang@apctp.org
†jojunghyo@apctp.org

contacts, respectively. The total contact energy of the system is then defined as

$$E = -\sum_{\langle ij \rangle} J_{\sigma_i \sigma_j}, \tag{1}$$

where $\sigma_i = \{\alpha,\beta\}$ represents the cell type at the ith site, and the bracket $\langle ij \rangle$ represents nearest neighbors. Note that $J_{\sigma_i\sigma_j}$ is the cell-to-cell contact energy between σ_i and σ_j. For example, when the system has total $N_{\alpha\alpha}$, $N_{\beta\beta}$, and $N_{\alpha\beta}$ contacts of α-α, β-β, and α-β, respectively, the total contact energy becomes

$$E = -(J_{\alpha\alpha}N_{\alpha\alpha} + J_{\beta\beta}N_{\beta\beta} + J_{\alpha\beta}N_{\alpha\beta}). \tag{2}$$

We are here interested in the regime of attractive interactions, i.e., $J_{\alpha\alpha}, J_{\beta\beta}, J_{\alpha\beta} > 0$. The frustration in the model originates from the competition between different cell-to-cell contacts. Our goal is to predict the spatial organization of binary cells that minimizes the total contact energy. In other words, given cellular composition (n_α, n_β) and interaction ($J_{\alpha\alpha}$, $J_{\beta\beta}$, $J_{\alpha\beta}$), we estimate the equilibrium structure represented by the order parameter, cell-to-cell contact numbers ($N_{\alpha\alpha}$, $N_{\beta\beta}$, $N_{\alpha\beta}$).

In the binary mixture model, two extreme states are easily expected. When the homotypic attractions $J_{\alpha\alpha}$ and $J_{\beta\beta}$ are dominant, homogeneous clustering of α cells and β cells appears. On the other hand, when the heterotypic attraction $J_{\alpha\beta}$ is dominant, heterogeneous mixing of alternating α and β cells appears. Indeed, the heterotypic contact $N_{\alpha\beta}$ shows a continuous transition from the sorting phase to the mixing phase as a function of the heterotypic interaction $J_{\alpha\beta}$. It has been suggested that the transition occurs at $J_{\alpha\beta} = (J_{\alpha\alpha} + J_{\beta\beta})/2$ [5]. At the critical condition, no preference to either sorting or mixing phase is anticipated. As an example of three α cells and three β cells in 1 dimension, an equivalent cell-to-cell contact energy is expected for the following two configurations: (i) $\alpha\alpha\alpha\beta\beta\beta$ and (ii) $\alpha\beta\alpha\beta\alpha\beta$, of which energy difference should be negligible as $2(J_{\alpha\alpha} + J_{\beta\beta}) - 4J_{\alpha\beta} = 0$. This simple argument gives the critical condition. Note that this argument is general beyond the 1-dimensional case.

In the 1-dimensional case, beyond the simple argument, we can exactly solve this problem using a partition function,

$$\mathcal{Z} = \sum_{\{\vec{\sigma}\}} e^{-E(\vec{\sigma})}, \tag{3}$$

where $\{\vec{\sigma}\}$ represents all possible sets of $\vec{\sigma} = (\sigma_1,\sigma_2,\ldots,\sigma_n)$ satisfying the constraint of cellular composition: n_α elements in the vector $\vec{\sigma}$ allocate $\sigma_i = \alpha$, and n_β ones allocate $\sigma_i = \beta$ with $n = n_\alpha + n_\beta$. The total contact energy in the system is simply determined by the number of homogeneous cell blocks. Depending on the number of boundaries between the homogeneous cell blocks, we decompose the partition function, $\mathcal{Z} = \mathcal{Z}_{\text{odd}} + \mathcal{Z}_{\text{even}}$, into odd and even ones:

$$\mathcal{Z}_{\text{odd}} = 2\sum_{k=0}^{k_{\max}} \binom{m_\alpha}{k}\binom{m_\beta}{k} \exp[-(m_\alpha - k)J_{\alpha\alpha} - (m_\beta - k)J_{\beta\beta} - (2k+1)J_{\alpha\beta}], \tag{4}$$

$$\mathcal{Z}_{\text{even}} = \sum_{k=0}^{k_{\max}} \left\{ \binom{m_\alpha}{k+1}\binom{m_\beta}{k} \exp[-(m_\alpha - k - 1)J_{\alpha\alpha} - (m_\alpha - k)J_{\beta\beta} - 2kJ_{\alpha\beta}] + \binom{m_\alpha}{k}\binom{m_\beta}{k+1} \exp[-(m_\alpha - k)J_{\alpha\alpha} - (m_\alpha - k - 1)J_{\beta\beta} - 2kJ_{\alpha\beta}] \right\}, \tag{5}$$

where $m_{\alpha,\beta} = n_{\alpha,\beta} - 1$ and $k_{\max} = \min\{m_\alpha, m_\beta\}$. After obtaining the partition function, it is straightforward to compute mean and variance of cell-to-cell contact numbers:

$$\langle N_{xy} \rangle = -\frac{1}{\mathcal{Z}}\frac{\partial \mathcal{Z}}{\partial J_{xy}}, \tag{6}$$

$$\delta N_{xy}^2 = \frac{1}{\mathcal{Z}}\frac{\partial^2 \mathcal{Z}}{\partial J_{xy}^2} - \langle N_{xy} \rangle^2, \tag{7}$$

where $x,y = \{\alpha,\beta\}$. Henceforth, we use the contact probabilities, $P_{xy} = \langle N_{xy} \rangle / N$, and its variance, $\delta P_{xy}^2 = \delta N_{xy}^2 / N^2$, normalizing the cell-to-cell contact numbers by total contact number, $N = N_{\alpha\alpha} + N_{\beta\beta} + N_{\alpha\beta}$. Using the analytical solution of the 1-dimensional partition function $\mathcal{Z}$, we confirm that the heterotypic association $P_{\alpha\beta}$ continuously increases as the heterotypic attraction $J_{\alpha\beta}$ increases. In addition, the fluctuation of the heterotypic association $\delta P_{\alpha\beta}^2$ has a single largest peak near the critical condition $(J_{\alpha\alpha} + J_{\beta\beta})/J_{\alpha\beta} \approx 2$. The exact value of $(J_{\alpha\alpha} + J_{\beta\beta})/J_{\alpha\beta}$, giving the largest fluctuation of the heterotypic association, depends on system size and cellular composition (n_α,n_β).

To explore binary mixtures in 3 dimensions, we use a Monte Carlo simulation because analytic calculation of the partition function in Eq. (3) above 2-dimensional lattices is intractable. Briefly explaining our algorithm, we (i) generate an initial cell configuration $\vec{\sigma}$ at random, satisfying the constraint, (n_α,n_β); (ii) randomly choose two cells to swap, and using Eq. (1), calculate the total contact energies of E and E' before and after exchanging the positions of the two cells; (iii) accept the exchange with the probability, $\min\{1, \exp(-\Delta E/T)\}$, where $\Delta E = E' - E$ and T denotes thermal energy, following the Metropolis algorithm [26,27]; and (iv) repeat this procedure until the system reaches equilibrium. We run several million Monte Carlo steps per cell for equilibrating and for averaging. Then we calculate the mean and variance of the cell-to-cell contact probabilities from the ensembles of several millions of microscopic states $\vec{\sigma}$. We found a good agreement between this numerical result with the above analytical results in Eqs. (6) and (7) in the 1-dimensional case. After validating our numerical method at least for the 1-dimensional case, we apply it to examine the self-organization of 3-dimensional islets. Since the biological system has a finite size, we simulated for sizes from $L \times L \times L = 10 \times 10 \times 10$ to $30 \times 30 \times 30$, corresponding to the size range of pancreatic islets. In addition, we used open boundary conditions because periodic boundary conditions are not appropriate; cells at opposite ends of the lattice cannot interact to each other in islets.

III. CELLULAR INTERACTION

Organ structure is determined by both cellular interactions and composition. We first examine the effect of cellular

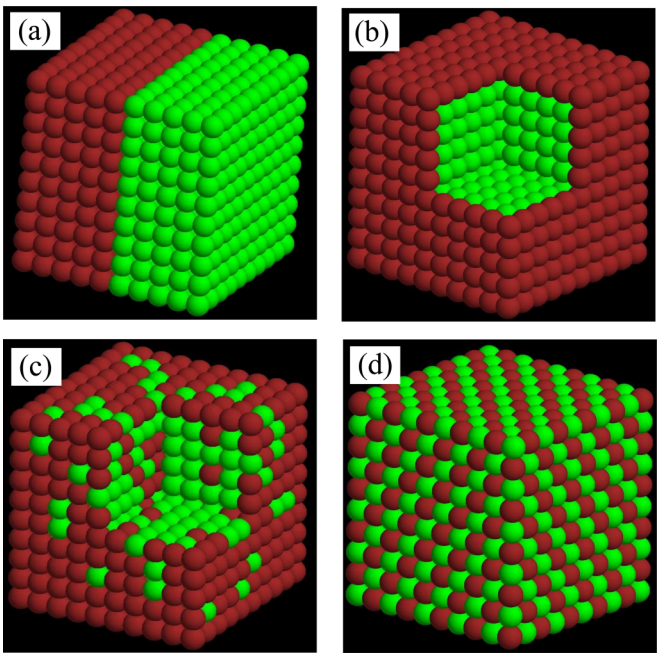

FIG. 1. (Color online) Organization of binary cells depending on cellular interaction. Cellular organizations of α [red (dark gray)] and β [green (light gray)] cells in a cubic lattice with a size $L = 10$: (a) complete sorting phase with a heterotypic attraction $J_{\alpha\beta} = 0.5$, (b) shell-core sorting phase with $J_{\alpha\beta} = 1.5$, (c) partial mixing phase with $J_{\alpha\beta} = 2.0$, and (d) complete mixing phase with $J_{\alpha\beta} = 3.5$, compared with homotypic attractions, $J_{\alpha\alpha} = 1$ and $J_{\beta\beta} = 3$. Thermal energy is $T = 0.5$, and fractions of each cell type are $p_\alpha = p_\beta = 0.5$. Note that we remove one edge of cubic lattices in (b) and (c) to show internal structures clearly.

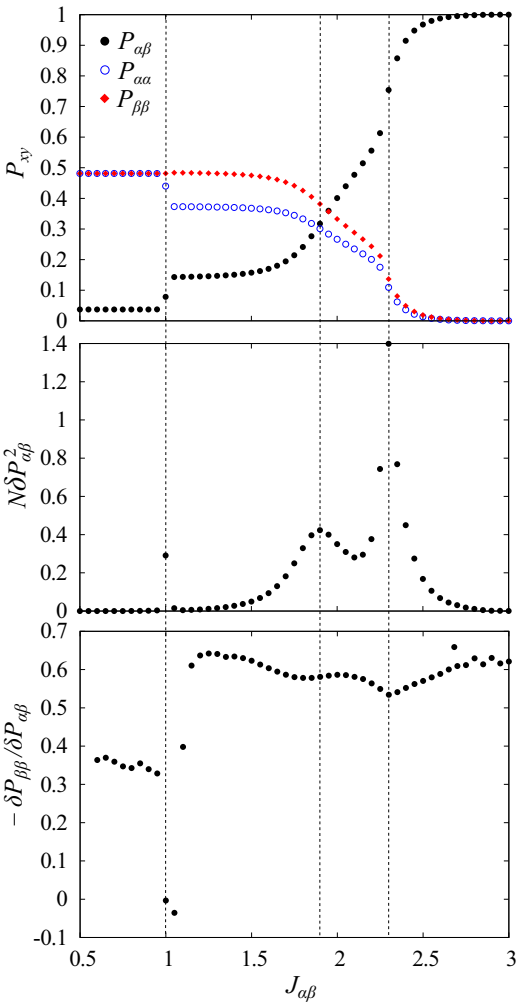

FIG. 2. (Color online) Cellular associations depending on heterotypic attraction. Cell-to-cell contact probabilities P_{xy} with $x, y = \{\alpha, \beta\}$: $P_{\alpha\alpha}$ (blue empty circle), $P_{\beta\beta}$ (red filled diamond), and $P_{\alpha\beta}$ (black filled circle) for α-α, β-β, and α-β contacts in the cubic lattice with $L = 10$; the fluctuation $\delta P^2_{\alpha\beta}$ of the α-β contact probability; and the difference ratio of $P_{\beta\beta}$ and $P_{\alpha\beta}$, $\delta P_{\beta\beta}/\delta P_{\alpha\beta} = (dP_{\beta\beta}/dJ_{\alpha\beta})/(dP_{\alpha\beta}/dJ_{\alpha\beta})$. For the simulation, we used homotypic attractions, $J_{\alpha\alpha} = 1$ and $J_{\beta\beta} = 3$, thermal energy, $T = 0.5$, and fractions of each cell type, $p_\alpha = p_\beta = 0.5$. Note that N is total number of cell-to-cell contacts. Dotted lines represent critical heterotypic attractions that show peaks for the fluctuation $\delta P^2_{\alpha\beta}$.

interactions. Given cellular composition (n_α, n_β), relative strengths of attractions between cell types govern cell-to-cell associations (Fig. 1). First, a weak heterotypic attraction ($J_{\alpha\beta} < J_{\alpha\alpha}, J_{\beta\beta}$) generates separate homogeneous clusters of α and β cells [Fig. 1(a)]. Second, a marginal heterotypic attraction ($J_{\alpha\alpha} < J_{\alpha\beta} < J_{\beta\beta}$) produces a shell-core structure composed of β cells in the core and α cells on the periphery [Fig. 1(b)]. Third, a little larger marginal heterotypic attraction ($J_{\alpha\alpha} \ll J_{\alpha\beta} < J_{\beta\beta}$) starts to mix two populations of cells, but yet preserves small clusters of homogeneous β cells [Fig. 1(c)]. Finally, a strong heterotypic attraction ($J_{\alpha\beta} > J_{\alpha\alpha}, J_{\beta\beta}$) results in complete mixture of alternating α and β cells [Fig. 1(d)]. For convenience, we call these four phases complete sorting, shell-core sorting, partial mixing, and complete mixing phases, respectively. As the heterotypic attraction increases, the heterotypic association $P_{\alpha\beta}$ grows, while the homotypic associations $P_{\alpha\alpha}$ and $P_{\beta\beta}$ diminish (Fig. 2). We observe four distinct phases depending on the heterotypic attraction $J_{\alpha\beta}$. At the boundaries between the phases, cellular associations show larger fluctuations, suggesting phase transitions (Fig. 2).

In the regime of $J_{\alpha\alpha} < J_{\alpha\beta} < (J_{\alpha\alpha} + J_{\beta\beta})/2$, the shell-core sorting phase has been proposed to appear [5]. Rather unexpectedly, however, we found that the distinct partial mixing phase exists between the shell-core sorting and complete mixing phase in the 3-dimensional binary mixture model. The new partial mixing phase shows subunits of homogeneous cell clusters. This phase becomes clearer in a larger lattice [Fig. 3(a)]. The critical heterotypic attractions $J^*_{\alpha\beta}$ decrease as increasing of system size; in particular, $J^*_{\alpha\beta}$ between the shell-core sorting and partial mixing phase decreases more significantly, compared with $J^*_{\alpha\beta}$ between the partial mixing and complete mixing phase [Fig. 3(b)].

Figure 4 is the phase diagram of our binary mixture model. It is of interest that the relative strengths of cellular attractions have linear relations at the phase boundaries. To understand its origin, we consider system energies at different phases (unprimed and primed):

$$E = -(J_{\alpha\alpha}N_{\alpha\alpha} + J_{\beta\beta}N_{\beta\beta} + J_{\alpha\beta}N_{\alpha\beta}), \tag{8}$$

$$E' = -(J_{\alpha\alpha}N'_{\alpha\alpha} + J_{\beta\beta}N'_{\beta\beta} + J'_{\alpha\beta}N'_{\alpha\beta}). \tag{9}$$

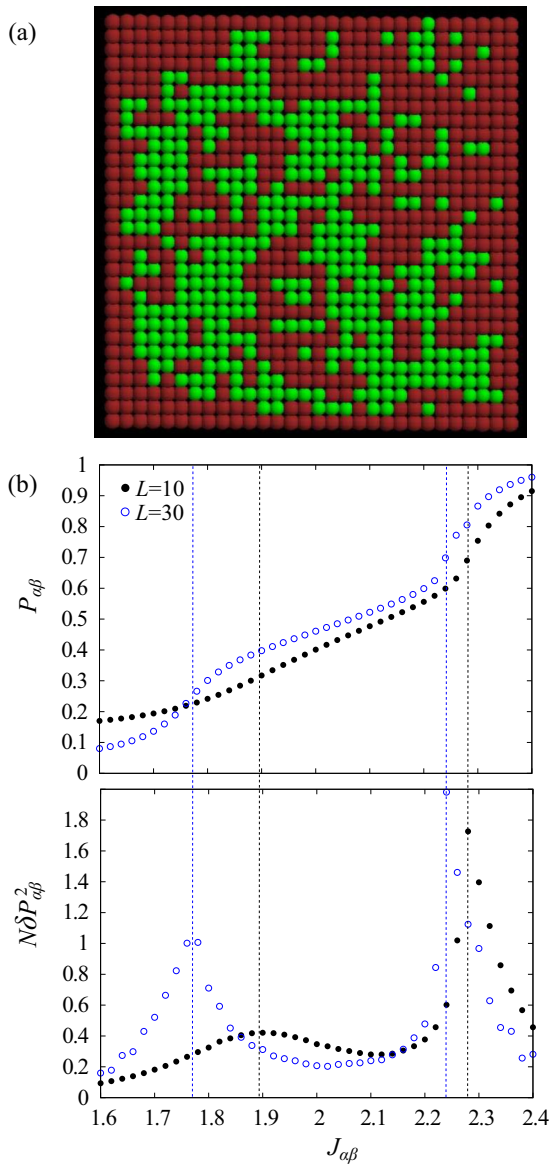

FIG. 3. (Color online) Partial mixing phase. (a) Cell arrangements in the binary mixture model for cellular interactions $J_{\alpha\alpha} = 1, J_{\beta\beta} = 3, J_{\alpha\beta} = 2$, thermal energy $T = 0.5$, α- and β-cell fractions $p_\alpha = p_\beta = 0.5$. For a clearer view of inner structure of the 3-dimensional cubic lattice with $L = 30$, we show a cut section. (b) Probability of α-β contacts and its fluctuation depending on heterotypic attraction $J_{\alpha\beta}$ with different sizes of cubic lattice: $L = 10$ (black filled circle) and $L = 30$ (blue empty circle). Note that N is total number of cell-to-cell contacts. Black and blue (dark and light gray) dotted lines represent critical heterotypic attractions at $L = 10$ and $L = 30$, respectively, that show peaks for the fluctuation $\delta P^2_{\alpha\beta}$.

As approaching to the critical interaction, $J^*_{\alpha\beta} = J_{\alpha\beta} = J'_{\alpha\beta}$, the two energies should converge as $E = E'$. Using that the total contact number is constant, $N = N_{\alpha\alpha} + N_{\beta\beta} + N_{\alpha\beta} = N'_{\alpha\alpha} + N'_{\beta\beta} + N'_{\alpha\beta}$, obtained is the following relation:

$$J^*_{\alpha\beta} = J_{\alpha\alpha} - \frac{\delta P_{\beta\beta}}{\delta P_{\alpha\beta}}(J_{\beta\beta} - J_{\alpha\alpha}), \tag{10}$$

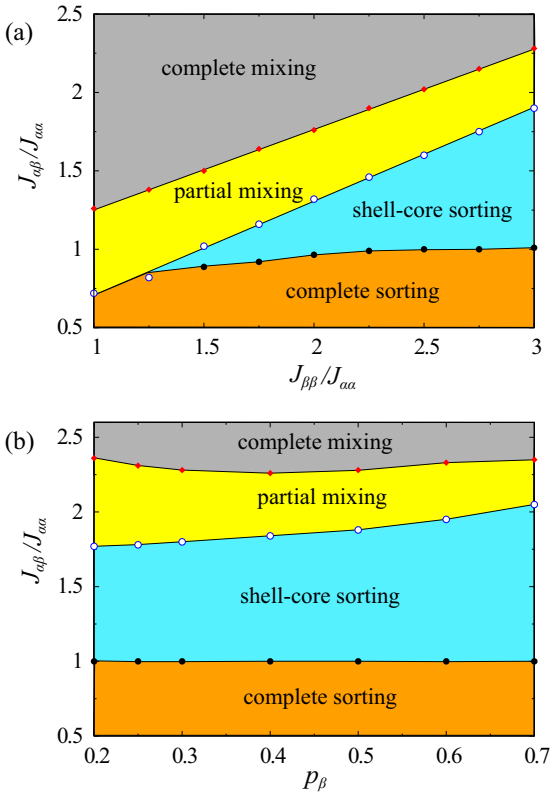

FIG. 4. (Color online) Phase diagram of the 3-dimensional binary mixture model. Depending on relative strengths of cellular interaction, complete sorting, shell-core sorting, partial mixing, and complete mixing phases arise. Thermal energy $T = 0.5$ is used in the cubic lattice with $L = 10$. (a) Phase diagram for $J_{\alpha\beta}/J_{\alpha\alpha}$ vs $J_{\beta\beta}/J_{\alpha\alpha}$, given fixed fractions of each cell type $p_\alpha = p_\beta = 0.5$. (b) Phase diagram for $J_{\alpha\beta}/J_{\alpha\alpha}$ vs β-cell fraction p_β, given fixed $J_{\alpha\alpha} = 1$ and $J_{\beta\beta} = 3$.

where $\delta P_{\beta\beta}/\delta P_{\alpha\beta} = (N'_{\beta\beta} - N_{\beta\beta})/(N'_{\alpha\beta} - N_{\alpha\beta})$. Indeed the values of $\delta P_{\beta\beta}/\delta P_{\alpha\beta}$ at the critical attractions $J^*_{\alpha\beta}$ in Fig. 2 explain the slopes 0.51 between the partial mixing and complete mixing phase, 0.60 between the shell-core sorting and partial mixing phase, 0.00 between the complete sorting and shell-core sorting phase Fig. 4(a). In particular, for the transition from the complete sorting to shell-core sorting phase, the number of β-β contacts changes negligibly, while the number of α-β contacts changes significantly (Fig. 2). Therefore, their phase boundary becomes $J^*_{\alpha\beta} \approx J_{\alpha\alpha}$ due to $\delta P_{\beta\beta}/\delta P_{\alpha\beta} \approx 0$ from Eq. (10). Finally, it should be noted that cellular composition can also govern the binary mixtures. Although cellular interactions are preserved, different cellular composition can show different cellular associations. In Fig. 4(b), given $J_{\alpha\beta}/J_{\alpha\alpha} = 2$ and $J_{\beta\beta}/J_{\alpha\alpha} = 3$, 50% β-cell fraction shows the partial mixing phase, while 70% β-cell fraction shows the shell-core sorting phase.

IV. CELLULAR COMPOSITION

Now we examine effects of cellular composition, finite size, and thermal fluctuations on the structure of binary mixtures. These effects are respectively discussed for distinct phases described in the previous sections.

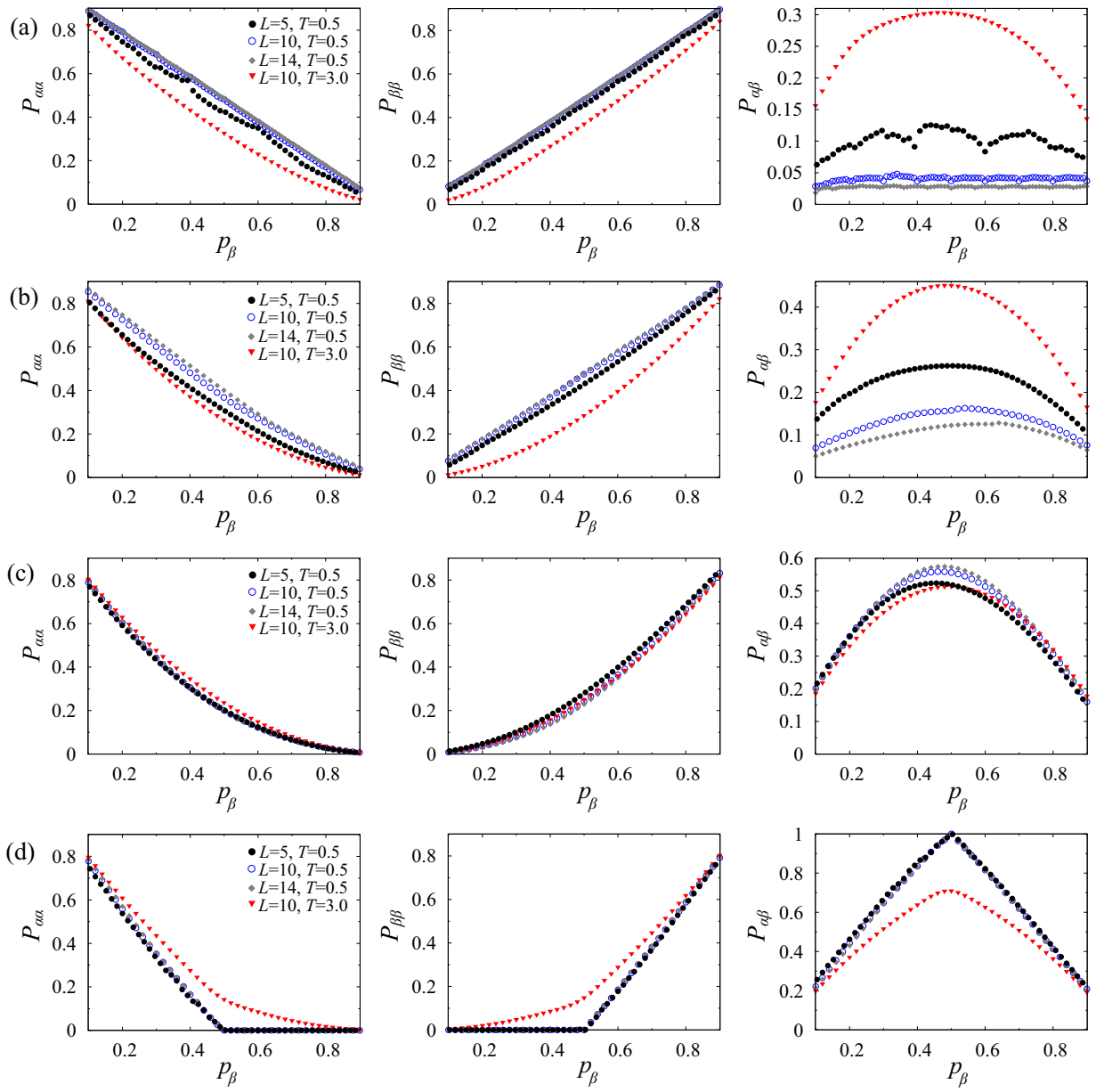

FIG. 5. (Color online) Cellular associations depending on cellular composition. Given homotypic attractions $J_{\alpha\alpha} = 1, J_{\beta\beta} = 3$, plotted are (a) complete sorting ($J_{\alpha\beta} = 0.5$), (b) shell-core sorting ($J_{\alpha\beta} = 1.5$), (c) partial mixing ($J_{\alpha\beta} = 2.2$), and (d) complete mixing ($J_{\alpha\beta} = 3.5$) phases. Three sizes of cubic lattice were used: $L = 5$ (black filled circle), $L = 10$ (blue empty circle), and $L = 14$ (gray diamond) under a thermal energy ($T = 0.5$). A higher thermal energy, $T = 3.0$ (red inverse triangle), was also considered with $L = 10$.

Complete sorting phase. When clustering of homogeneous cells is favored, the boundary between the two clusters is the only source for the heterotypic cell contact. In cubic lattices, therefore, as the β-cell fraction increases, the heterotypic cell association $P_{\alpha\beta}$ does not change much, while the homotypic cell associations $P_{\alpha\alpha}$ and $P_{\beta\beta}$ linearly decrease and increase, respectively [Fig. 5(a)]. In a cubic lattice ($L \times L \times L$), when the cell fraction becomes $p_\beta = m/L(=mL^2/L^3)$ with integer $m = \{1,2,\ldots,L-1\}$, the boundary area between the two cuboid clusters of homogeneous cell types is minimal. This causes the multimodal minimum of $P_{\alpha\beta}$ [Fig. 5(a)]. This multimodality, however, disappears under a higher thermal fluctuation.

Shell-core sorting phase. When the heterotypic attraction roughly satisfies $J_{\alpha\alpha} < J_{\alpha\beta} < (J_{\alpha\alpha} + J_{\beta\beta})/2$, the shell-core sorting phase emerges with the β-cell core enveloped by α cells. The shell-core sorting phase shows homotypic cell associations similar to those of the complete sorting phase where $P_{\alpha\alpha}$ or $P_{\beta\beta}$ linearly increase with respect to p_α or p_β [Fig. 5(b)]. The linear behavior disappears under a higher thermal fluctuation. However, the heterotypic cell association shows a rounded maximum $P^*_{\alpha\beta}$ at a critical fraction p^*_β, unlike the constant $P_{\alpha\beta}$ in the complete sorting phase. The critical fraction p^*_β and the maximum heterotypic association $P^*_{\alpha\beta}$ depend on system size: as lattice size increases, p^*_β increases, while $P^*_{\alpha\beta}$ decreases. In the shell-core sorting

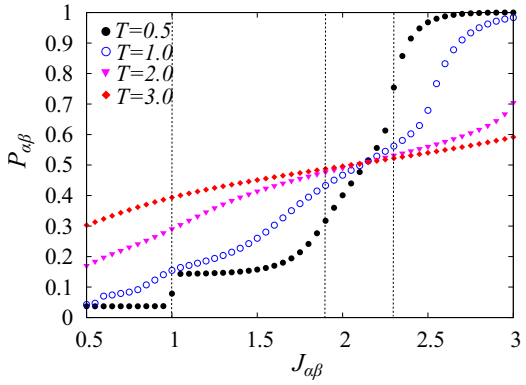

FIG. 6. (Color online) Robustness under thermal fluctuations. Heterotypic association is plotted as a function of heterotypic attraction $J_{\alpha\beta}$. Homotypic attractions $J_{\alpha\alpha} = 1$ and $J_{\beta\beta} = 3$ and fractions of each cell type, $p_\alpha = p_\beta = 0.5$ used in the binary mixture model of $L = 10$ cubic lattice. Different temperature energies were compared: $T = 0.5$ (black filled circle), $T = 1.0$ (blue empty circle), $T = 2.0$ (magenta inverse triangle), and $T = 3.0$ (red diamond). Dotted lines represent critical attractions dividing distinct phases in the binary mixture.

phase, the heterotypic association can be maximized when the boundary surface between the core β-cell cluster and the α-cell shell becomes largest. In the cubic lattice ($L \times L \times L$), this situation is realized when β cells occupy the cubic lattice of size $(L-2)^3$ in the core, and α cells occupy the six surfaces of the cubic lattice. Thus, the critical β-cell fraction is given by $p^*_\beta = (1-2/L)^3$. It increases as the lattice size L increases: $p^*_\beta(L=10) = 0.51$ and $p^*_\beta(L=14) = 0.63$. We also calculate the maximum heterotypic association in this case. The cubic lattice has total $N = 3(L^3 - L^2)$ cell contacts. Among them, the number of heterotypic contacts is $N^*_{\alpha\beta} = 6(L-2)^2$. It gives the heterotypic association, $P^*_{\alpha\beta} = N^*_{\alpha\beta}/N = 2(1-2/L)^2/(L-1)$. When lattice size is large ($L > 3+\sqrt{5}$), the heterotypic association decreases with lattice size: $P^*_{\alpha\beta}(L=10) = 0.14$ and $P^*_{\alpha\beta}(L=14) = 0.11$. Note that the actual $p^*_\beta(L=10) = 0.54$ and $p^*_\beta(L=14) = 0.64$ are a little larger than the predicted ones [Fig. 5(b)]. In addition, the actual $P^*_{\alpha\beta}(L=10) = 0.16$ and $P^*_{\alpha\beta}(L=14) = 0.13$ are a little larger than the predicted ones, because the appearance of a few β cells on the pure α-cell shell can further increase the heterotypic association.

Partial mixing phase. The partial mixing phase exists between the shell-core and complete mixing phase. One noteworthy feature is that cellular associations in the partial mixing phase are tolerant to changes of thermal fluctuations, compared with the ones in other phases [Fig. 5(c)]. In particular, a specific heterotypic attraction $J_{\alpha\beta} = 2.15$ with $J_{\alpha\alpha} = 1$ and $J_{\beta\beta} = 3$ does not change cellular associations for different thermal fluctuations (Fig. 6).

Complete mixing phase. When the heterotypic interaction $J_{\alpha\beta}$ is dominant, alternation of α and β cells is favored. Therefore, homotypic cell associations are prevented until one population of cells occupies more than half fraction. This explains the sharp transitions at $p_\alpha = p_\beta = 0.5$ [Fig. 5(d)]. The complete mixing phase has negligible finite size effects, compared with other phases.

V. SUMMARY

We studied the binary mixture on the cubic lattice. Depending on the relative attractions between cell types, we observed four distinct phases: complete sorting, shell-core sorting, partial mixing, and complete mixing phase. Glazier and Graner has also observed these four phases in the extended 2-dimensional Potts model with the sub-cellular lattice [12,13]. In this study, we demonstrated that these four phases are clearly separate based on the large fluctuation of cellular associations at the boundaries between them, representing phase transitions. It is of particular interest that the partial mixing phase distinctively exists between the shell-core sorting and complete mixing phase. It is noteworthy that the previous studies, based on the subcellular lattice model, have observed the partial mixing phase as a transient phase changing from the complete mixing phase to the shell-core sorting phase [11–13]. However, our simulation, based on the simple cellular lattice model, verified that the partial mixing phase is an equilibrium phase at special differential cell adhesions. The partial mixing phase has been named previously the *partial sorting phase* [12,13]. Sorting and mixing are two aspects of a single phenomenon. Cell sorting has been extensively studied to examine the sorting condition and kinetics [9–11,15,28]. However, cell mixing has not been emphasized much, although the organized mixing of heterotypic cells is expected to play a crucial role for their cellular interactions.

The partial mixing phase had a very special feature that cellular associations at the unique phase were extremely robust to thermal fluctuations. The phase consisted of several subdivisions of the shell-core structures of binary cells. The pattern showed a great similarity to large (>100 μm diameter) human islets [25].

It is of interest that pancreatic islets, consisting of mainly α and β cells, have similar size ranges, but different structures between species [22,24]. Mouse and rat islets show the shell-core sorting phase, while human islets show the partial mixing phase. Both cellular interactions and composition can originate the structural differences. Unlike binary mixture models usually considered in physics, cellular composition and finite size effect are important factors to consider in biological systems [10,15]. It has been observed that human islets have a higher fraction of α cells, 20%–40%, compared with 10%–20% in mouse islets [22]. The present study suggested the possibility that the different cellular composition could drive different structures of mouse and human islets, although their cellular interactions were preserved. However, since the relative attractions between the endocrine cells have not been measured yet, it is not clear whether the different islet structures originate from their different cellular composition, different cellular interactions, or both. Dissociated rat islet cells spontaneously aggregate and form pseudoislets, similar to native rat islets [29]. This pseudoislet formation proposes an intriguing experiment whether dissociated mouse islet cells form the human islet structure by increasing their α-cell composition, or dissociated human islet cells form the mouse islet structure by decreasing their α-cell composition.

It has been reported that different endocrine cells express different cell adhesion molecules [30]. The distinct strengths

of relative attraction between cell types can provide the physical mechanism of the self-organization of islet structures [31]. Here, thermal fluctuations could provide motility of cells during their self-organization process, and their strength relative to the cell-to-cell attraction affected equilibrium structures of islets. It has been proposed that under pathological conditions, the islets could flexibly change their structures to meet corresponding metabolic demands [32]. Perturbed expression of cell adhesion molecules can be a potential mechanism for the structural changes.

ACKNOWLEDGMENTS

We are grateful to anonymous reviewers for useful comments. We thank Marissa Pastor for a critical reading of the manuscript. This research was supported by the Basic Science Research Program through the National Foundation of Korea funded by the Ministry of Science, ICT, and Future Planning (No. 2013R1A1A1006655) and by the Max Planck Society, the Korea Ministry of Education, Science, and Technology, Gyeongsangbuk-Do, and Pohang City.

[1] K. Huang, *Statistical Mechanics* (John Wiley & Sons, New York, 1987), Chap. 14.
[2] M. M. de Oliveira and R. Dickman, Phys. Rev. E **84**, 011125 (2011).
[3] M. Matsuo, J. Phys. Soc. Jpn. **71**, 1011 (2002).
[4] H. Noguchi, J. Chem. Phys. **138**, 024907 (2013).
[5] M. S. Steinberg, Science **141**, 401 (1963).
[6] C. P. Beatrici and L. G. Brunnet, Phys. Rev. E **84**, 031927 (2011).
[7] P. Armstrong, Crit. Rev. Biochem. Mol. Biol. **24**, 119 (1989).
[8] A. Mochizuki, Y. Iwasa, and Y. Takeda, J. Theor. Biol. **179**, 129 (1996).
[9] R. Takano, A. Mochizuki, and Y. Iwasa, J. Theor. Biol. **221**, 459 (2003).
[10] J. C. M. Mombach, Phys. Rev. E **59**, R3827 (1999).
[11] E. Flenner, L. Janosi, B. Barz, A. Neagu, G. Forgacs, and I. Kosztin, Phys. Rev. E **85**, 031907 (2012).
[12] J. A. Glazier and F. Graner, Phys. Rev. E **47**, 2128 (1993).
[13] F. Graner and J. A. Glazier, Phys. Rev. Lett. **69**, 2013 (1992).
[14] P. Hogeweg, J. Theor. Biol. **203**, 317 (2000).
[15] M. S. Hutson, G. W. Brodland, J. Yang, and D. Viens, Phys. Rev. Lett. **101**, 148105 (2008).
[16] M. Emily and O. Franois, Theor. Biol. Med. Modell. **4**, 1 (2007).
[17] G. W. Brodland, Appl. Mech. Rev. **57**, 47 (2004).
[18] D. Drasdo, R. Kree, and J. S. McCaskill, Phys. Rev. E **52**, 6635 (1995).
[19] S. Turner, J. A. Sherratt, K. J. Painter, and N. J. Savill, Phys. Rev. E **69**, 021910 (2004).
[20] A. Caicedo, Semin. Cell. Dev. Biol. **24**, 11 (2013).
[21] D. S. Koh, J. H. Cho, and L. Chen, J. Mol. Neurosci. **48**, 429 (2012).
[22] A. Kim, K. Miller, J. Jo, G. Kilimnik, P. Wojcik, and M. Hara, Islets **1**, 129 (2009).
[23] M. Brissova, M. J. Fowler, W. E. Nicholson, A. Chu, B. Hirshberg, D. M. Harlan, and A. C. Powers, J. Histochem. Cytochem. **53**, 1087 (2005).
[24] O. Cabrera, D. M. Berman, N. S. Kenyon, C. Ricordi, P.-O. Berggren, and A. Caicedo, Proc. Natl. Acad. Sci. USA **103**, 2334 (2006).
[25] D. Bosco, M. Armanet, P. Morel, N. Niclauss, A. Sgroi, Y. D. Muller, L. Giovannoni, G. Parnaud, and T. Berney, Diabetes **59**, 1202 (2010).
[26] N. Metropolis and S. Ulam, J. Am. Stat. Assoc. **44**, 335 (1949).
[27] M. E. J. Newman and G. T. Barkema, *Monte Carlo Methods in Statistical Physics* (Oxford University Press, New York, 2001).
[28] J. M. Belmonte, G. L. Thomas, L. G. Brunnet, R. M. C. de Almeida, and H. Chaté, Phys. Rev. Lett. **100**, 248702 (2008).
[29] P. A. Halban, S. L. Powers, K. L. George, and S. Bonner-Weir, Diabetes **36**, 783 (1987).
[30] C. Kelly, H. G. Parke, J. T. McCluskey, P. R. Flatt, and N. H. McClenaghan, Diabetes Metab. Res. Rev. **26**, 525 (2010).
[31] D. Jia, D. Dajusta, and R. A. Foty, Dev. Dyn. **236**, 2039 (2007).
[32] D. J. Steiner, A. Kim, K. Miller, and M. Hara, Islets **2**, 135 (2010).